Materials and Design 195 (2020) 108964

Contents lists available at ScienceDirect

Materials and Design

journal homepage: www.elsevier.com/locate/matdes

Tailored bainitic-martensitic microstructures by means of inductive surface hardening for AISI4140

F. Mühl *, J. Jarms, D. Kaiser, S. Dietrich, V. Schulze

Institute of Applied Materials (IAM-WK), Karlsruhe Institute of Technology (KIT), Karlsruhe, Germany

HIGHLIGHTS

- Innovative concept for the inductor that enables a cooling with compressed air during induction hardening.
- Investigations of bainitic phase transformation after short time austenitization.
- Development different heat treatment strategies creating bainitic-martensitic microstructures by means of induction hardening.
- Improvement of the surface layer state of induction hardened parts.

GRAPHICAL ABSTRACT

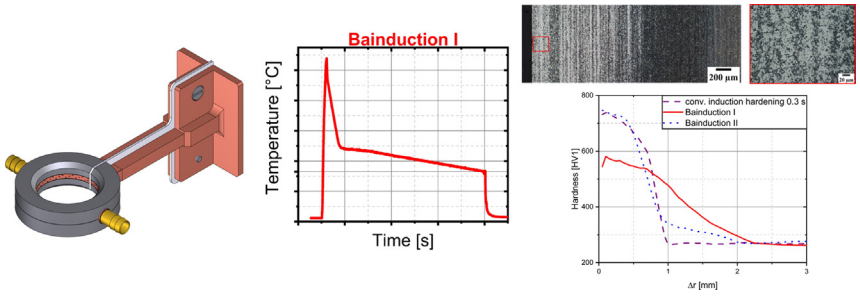

ARTICLE INFO

Article history:
Received 18 May 2020
Received in revised form 30 June 2020
Accepted 8 July 2020
Available online 15 July 2020

Keywords:
Induction hardening
Heat treatment
Bainite/martensite dual phase
Residual stresses
Mechanical properties
Steel treatment

ABSTRACT

Inductive surface hardening processes are widely used in the manufacturing of automotive parts. They combine short process times with high economic and energy efficiency. Because of their high surface hardness, induction hardened steel parts feature beneficial wear resistance and also good fatigue properties due to the induced compressive residual stresses in the surface. Considering the positive effects on the mechanical properties by creating a bainitic-martensitic microstructure, outlined by severel authors, this study includes the implementation of a temperature controlled inductive surface hardening process on a conventional hardening machine. Therefore an innovative inductor design, which allows a controlled sample cooling is presented. Supported by dilatometric studies as well as different heat treatment strategies, limitations are identified to gain a profund process understanding. Hereby an accelerated bainite formation after short time austenitization is detected. By using different heat treatment strategies, the fraction of the bainitic phase can be adjusted in the surface of the part made of AISI 4140. The results of this innovative heat treatment method are compared to short time inductive hardening and tempering processes regarding microstructure, hardness and residual stresses. The generated surface layer states, including mixed microstructures, show promising properties resulting in a possible enhancement of the fatigue strength of induction hardened parts.

1. Introduction

1.1. Motivation

Induction hardening is a widely used steel heat treatment process in the manufacturing of components as gears and crankshafts due to its positive impact on both tribological and fatigue properties. Moreover, the process causes less warpage than conventional heat treatment methods and reduces the risk of crack formation. Further advantages are a high degree of automation and good controllability. [1–4]

Fig. 1a depicts a typical surface layer state after induction hardening showing high compressive residual stresses and high hardness values directly at the surface. It can be seen that the transition from the hardened case towards the untreated core of the component usually occurs abruptly. Therefore, hardness and residual stresses are altering

* Corresponding author.
E-mail address: fabian.muehl@kit.edu (F. Mühl).

https://doi.org/10.1016/j.matdes.2020.108964

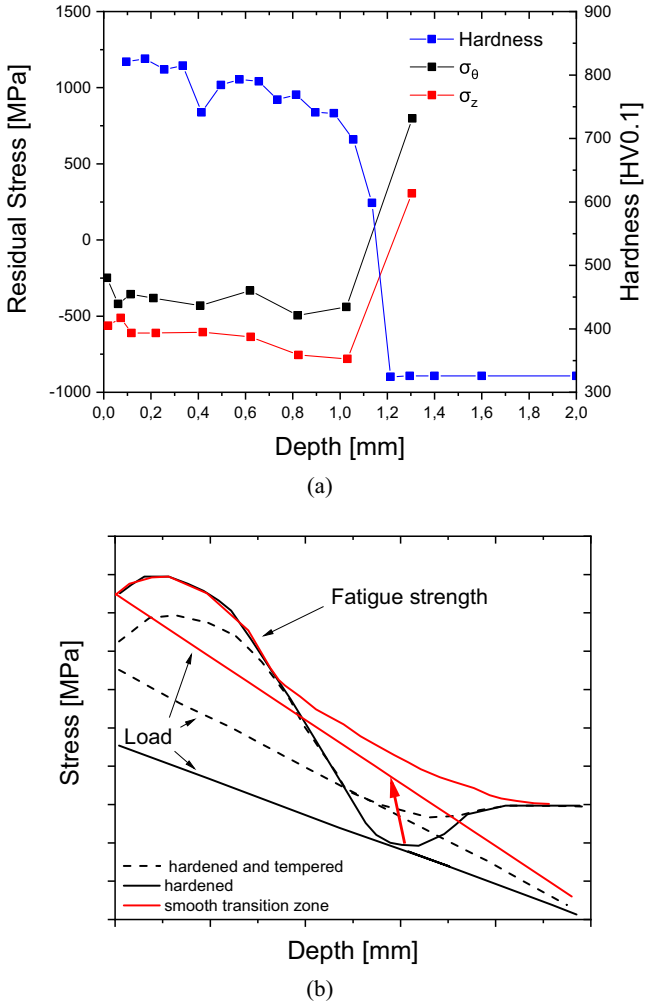

Fig. 1. Surface layer state after induction hardening [10] (a) and illustration of the resulting fatigue strength compared to the loading stresses [9] (b).

drastically in the transition zone [5]. High tensile residual stresses in this transition zone as well as in the region of the unaffected microstructure can have a negative influence on the fatigue behaviour of induction hardened parts. In the work of Komotori et al. [6] it was shown that depending on the hardening depth and load case the crack initiation during cyclic loading can occur in these inner critical sections. Furthermore, in the case of a low tempered initial microstructure, the formation of a local minimum of hardness caused by unintended tempering effects during induction heating is observed [7,8]. These high tempered sections below the hardened surface layer impairs the fatigue behaviour of induction hardened components as the strength is reduced. Short heating times counteract the tempering effects but also lead to thinner hardened layers and the mentioned abrupt drop of hardness limiting the load case. The effect of a smooth transition zone on the fatigue strength is indicated in Fig. 1 and shows high potential enabling higher loading stresses of induction hardened parts.

Overall tensile residual stresses coupled with a weakening of the initial microstructure in the transition zone of induction hardened parts are critical factors in the design of components. Braisch et al. [9] showed, that a subsequent tempering process, decreasing the tensile residual stresses, can have positive effects on the fatigue strength (see Fig. 1b). However the abrupt transition of strength to the weaker initial microstructure is still limiting the potential of induction hardend steel components.

In contrast, mixed microstructures of bainite and martensite show a rise in tensile strength as well as increased ductility up to 25% V_b (volume fraction of bainite) [11,12]. There are two factors influencing the mechanical properties of bainitic and martensitic microstructures described by Young et al. [13]. On the one hand the formation of bainite increases the strength of martensite due to the enrichment of carbon in the residual austenite. On the other hand especially at low volume fractions the strength of bainite is enhanced by plastic constraint effects. Here it is assumed that a elongation of bainite is limited by the surrounding rigid martensite. The influence of mixed microstructures on the fatigue behaviour was investigated by Chen et al. [14]. Their findings confirm the results of [11], showing the highest fatigue strength at bainite contents between 21% and 49%. Especially the formation of lower bainite by austempering processes improves the mechanical properties [15,16]. Taking these effects and resulting properties into account, the generation of a mixture of bainite and martensite in the stated transition zone is a promising approach optimizing its mechanical properties. In addition, a surface layer containing tailored bainitic-martensitic mixtures in instead of the conventional martensitic microstructure enables the creation of high strength surface states with enhanced ductility.

1.2. This work

This work presents an innovative heat treatment process, termed *Bainduction*, generating a mixed microstructure of bainite and martensite in surface layers or in the transition zone between the hardened surface and the initial microstructure of induction hardened surfaces. By creating a smoothly graded microstructure with decreasing V_M (volume fraction of martensite), a continuous transition between the case and core hardness can be attained. The *Bainduction* experiments are supported by dilatometric tests with subsequent metallographic examinations and hardness measurements to provide information about the bainite formation after short time austenitization and the resulting microstructure after different heat treatment strategies. Furthermore an electromagnetic FE-model was used to estimate internal temperatures and the heat transfer at the surface during the process. For the experimental implementation of the described heat treatment routes a controlled cooling in the temperature range where the formation of bainite is expected must be realized. For that reason a conventional induction hardening machine was modified with a newly developed innovative inductor concept to allow these heat treatments. By using this concept the work investigates different heating and cooling parameters during induction hardening of ring-shaped samples and their effects on the surface layer state. This is done by analysing the microstructure, hardness and the residual stress state in the surface.

2. Materials and methods

2.1. Test material

The shown experiments were carried out with the low alloyed steel AISI4140 (german grade 42CrMo4) in a quenched and tempered state. The initial hardness of the batch used for the induction heat treatments was 275 HV. The dilatometric tests were executed with a different batch. The chemical composition of the two investigated batches are listed in Table 1 respectively.

Table 1
Chemical compositions of the used steels batches.

	C	Si	Mn	Cr	Mo	Fe
Dilatometry	0.42	0.22	0.69	0.94	0.19	bal.
Induction hardening	0.44	0.22	0.71	0.96	0.16	bal.

2.2. Dilatometry

The dilatometric investigations were carried out with the push rod dilatometer DIL 805 by TA Instruments. Cylindrical, hollow specimens (length: 10 mm, diameter: 4 mm, wall thickness: 1 mm) were used for the experiments. The controlled heating was realized by induction heating using a Type S thermocouple in the center of the sample. The length change of the specimens was measured with an inductive displacement transducer during the experiments.

All specimens were heated up to 1000 °C in 1 s and then directly cooled to the quenching temperatures T_Q 500 °C and 600 °C, respectively. After that, they are slowly cooled down to the martensite start temperature M_s within different cooling times t_{cool}, which vary between 30 s and 75 s. Hereby mixtures with different bainitic phase fractions V_b were generated. M_s was estimated with the formula given in [17]. To compare the results and to assess the influence of short time austenitisation, two specimen were also heated within 60 s and then cooled down similarly with a cooling time of 30 s. Fig. 2 shows the different measured temperature curves of the investigated heat treatments. It has to be stated that the cooling rate of 1000 Ks^{-1} can only be achieved up to the AC_1 temperature due to the arising latent heat. The resulting averaged heating rate is around 860 Ks^{-1}. The resulting microstructures are then characterized by hardness measurements and optical microscopy of the crosssection in the center of the sample.

2.3. Induction hardening experiments

Fig. 3 shows the ring-shaped specimens used in the *Bainduction* experiments. The location of the heat affected surface layer by the inductor is marked red. The blue arrow shows the position of the welded thermocouple (Type K).

The Bainduction experiments were conducted with the FIAND KHM 750 hardening machine using an IDEA SMS850 dual-frequency converter. The genererator of the hardening machine allows a simultaneous dual frequency inductive heat treatment with a maximum power output of 850 kW and frequency bands of 10 — 30 kHz for the MF and 150 — 450 kHz for the HF mode. However, its power output cannot be controlled by the temperature in the surface layer of the specimens. To allow a controlled cooling, a machine integrated quench (MIQ) inductor was designed (Fig. 4) enabling a cooling with compressed air. The inductor was realized via laser powder bed fusion due to the better producibility compared to machining, omitting conventional brazing, bending and machining steps. The electrical properties of additively

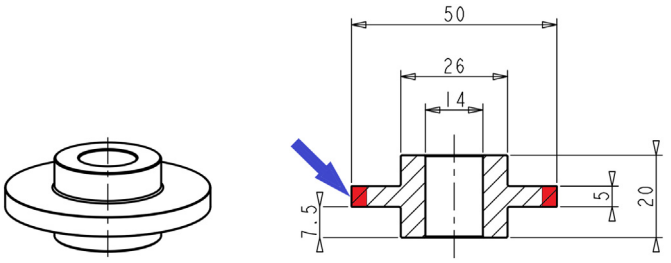

Fig. 3. Geometry of the ring-shaped specimen used for Bainduction heat treatments (mm).

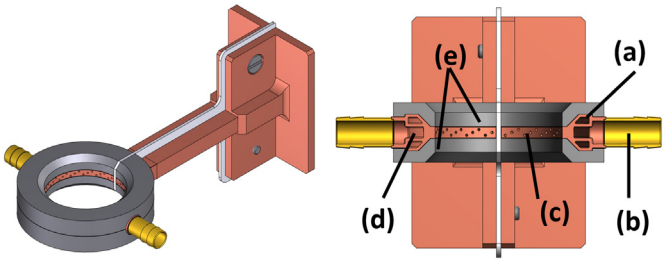

Fig. 4. Concept of the used inductor: (a) cooling water circuit, (b) compressed air supply, (c) air nozzle, (d) air channel, (e) field concentrator.

manufactured inductors similar to the one used in this work were investigated in [18]. Here it was shown that almost the same electrical conductivity compared to the bulk material can be achieved by a subsequent heat treatment of the additively manufactured inductors. The used inductor has two cooling water channels to prevent the inductor from overheating and a compressed air channel for quenching. Hereby the compressed air can flow through nozzles on the inside of the inductor onto the surface of the specimen causing a rapid cooling effect and a controlled cooling over several seconds can be realized by simultaneous low power heating during compressed air cooling.

The complete experimental setup is shown in Fig. 5. The air supply system is connected with a proportinal air valve allowing a controlled cooling of the surface. Due to the fact that the temperature is controlled using a welded thermocouple a rotation of the sample was disabled during the experiments. During the experiments the surface of the specimen was heated to 1000 °C in 1 s by using 13.5% of the total MF-power, which corresponds to a power of 54 kW. Meanwhile, the controller of the air cooling system is suspended until the surface of the specimen

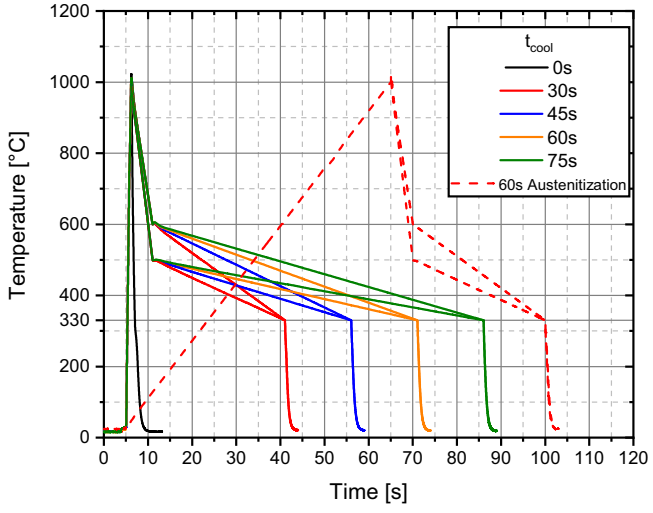

Fig. 2. Measured temperature profiles of the heat treatment strategies after short-time austenitisation.

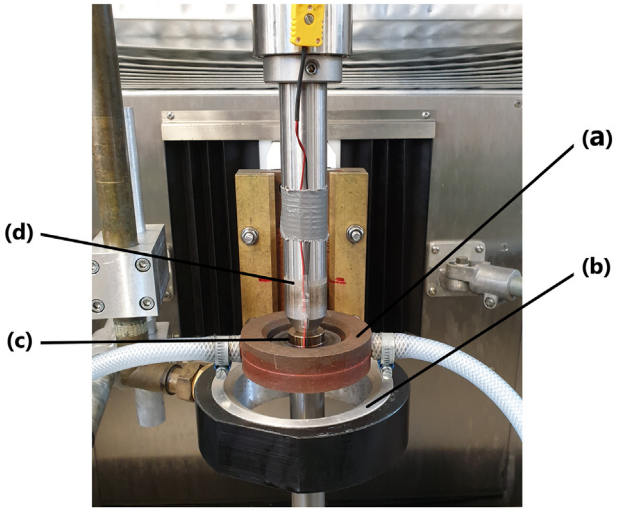

Fig. 5. Experimental setup: (a) inductor with compressed air supply, (b) quenching shower, (c) sample with thermocouple, (d) tailstock.

reaches the required temperature of 1000 °C. Then, the controlled cooling takes over and the sample can be cooled down to the desired temperature by self-quenching effects and the air cooling system. To realize low cooling rates and therefore the formation of bainite (see Fig. 2), the surface layer is heated simultaneously with a constant low power (2 − 3.2 kW). After reaching M_S the specimen are either directly quenchend by a water-polymer-mixture spray (*Bainduction I*) or reaustenitized with HF-power (115 kW) followed by a quenching step (*Bainduction II*). Furthermore, an alternative heat treatment route where the re-austenitization takes place after quenching is tested (*Bainduction III*). This was done with a HF-Power of (90 kW). In all experiments the used frequencies were 15 KHz for MF and 255 kHz for HF respectively. The three described heat treatment strategies Bainduction I-III are schematically visualized in Fig. 6. The basic principle of the first method is to realize a mixed microstructure directly in the surface layer improving the mechanical properties (see Section 1). The other two strategies aim at smoothing of the hardness development as well as strengthening of the transition zone, where tensile residual stresses arise in the conventional induction hardening process. Additionally, induction hardening experiments were carried out to compare the generated surface layer states with a purely martensitic surface. Here the samples were heated up in 0.3 s as well as in 0.075 s to 1000 °C with a HF-power of 40 kW and 99 kW respectively and subsequently quenched by the spray.

2.4. Metallographic characterization and residual stress measurements

2.4.1. Metallographic characterization

The heat treated samples were cut in axial direction as shown in Fig. 7 and the resulting longitudinal crosssection embedded, grinded and polished up to 3μm. The subsequent hardness measurements were done with a Qness Q10A hardness tester and a testing load of 10 N. To achieve a high resolution of the hardness developement in the surface, a measurement path as shown in Fig. 7 was chosen. The minimum distance between two measured points is 250μm. Hereby the requirements of the DIN EN ISO 6507-1 standard [19] are fulfilled. For the investigation of the microstructure the samples were polished up to 0.04μm and etched with 2% Nital etch.

2.4.2. Residual stress measurements

The depth resolved residual stress analyes of an uncut sample was performed in the center of the outer surface. The analyses were carried out by sequential electro chemical material removal using the STRUERS LectroPol-5 polishing device. The residual stresses in axial as well as in tangential direction were determined using the X-ray diffraction method $\sin^2(\psi)$ with $E_{211} = 219911$ MPa and $\nu_{211} = 0.28$ [20]. A

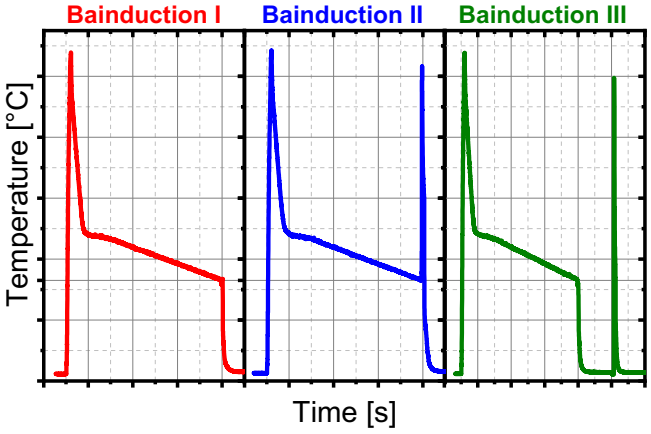

Fig. 6. Schematical overview of the Bainduction heat treatment strategies.

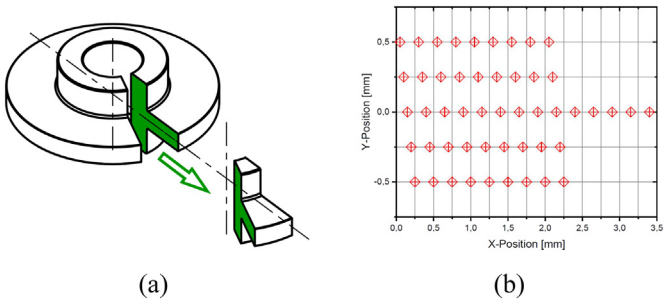

Fig. 7. Metallographic investigated longitudinal crosssection (a) and the hardness measuring path (b).

ψ-diffractometer and V-filtered CrK_α radiation were used to measure the {211} α-Fe diffraction line at 15 ψ angles between −60° and 60°. Hereby the primary beam is collimated using a pinhole with a diameter of 1 mm. On the secondary side a scintillation counter with a 4 mm symmetrizing slit was used.

2.5. FE-model

In order to obtain more information about the process parameter and the temperature developement in the interior of the sample, the heat treatment, considering the electromagnetic and thermal processes, was simulated. Based on the FE-model in [7] a 2.5D half-model with axial symmetry around the z-axis as shown in Fig. 8 was regarded. The dimensions are equivalent to those shown in Fig. 3. Here C3D8T and EMC3D8 elements were used for the thermal and the electromagnetic model respectively. The simulation was performed using Abaqus/Standard and Abaqus/Electromagnetic with the thermal and electromagnetic material properties of AISI4140 and boundary conditions given in [7]. It has to be stated that the latent heat was neglected in the simulative consideration. The used frequency corresponds to the one recorded during the experimentally conducted induction hardening tests. Based on the validated electromagnetic model shown in [10] the implemented currents were adjusted to the experimentally measured temperatures. In the range of the controlled heat treatment step with a constant low MF-Power the air cooling was modeled using a heat transfer on the surface with a heat transfer coefficient.

3. Results

3.1. Analysis of the dilatometric experiments

Figs. 9 and 10 depict the measured length change signal versus the temperature after short time austenitization of the presented heat treatments in Fig. 6. After quenching to 500 °C (Fig. 9), a significant change of the length due to bainite transformation can be detected for all cooling times. Reaching 330 °C all measured curves show a small kink because of the shift to fast quenching without induction heating down to room temperature. In the case of the shortest cooling time of 30 s a difference of the length change induced the a martensitic transformation can be observed. This change gets very small with increasing cooling time, indicating a nearly full bainitic microstructure. Comparing the martensite start temperature after the cooling time of 30 s with the determined value after direct quenching down to room temperature ($t_{cool} = 0\ s$) a shift of M_s to lower temperatures can be detected. This indicates a carbon enrichment in the residual austenite during bainite formation. With increasing quenching temperature this effect gets stronger (see Fig. 10) on the basis of an enhanced carbon diffusion at higher temperatures. Here the increasing volume due to martensite formation is also visible after cooling times of 45 s and 60 s. So less bainite is transformed during a slow cooling from 600 °C in comparison to 500 °C, which can be

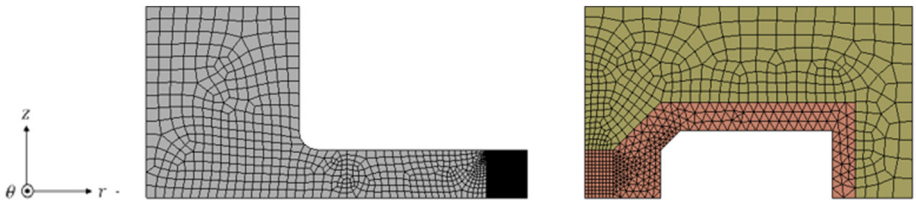

Fig. 8. FE-model of the ring shaped sample: sample (grey), inductor (copper colored) and field concentrator (yellow).

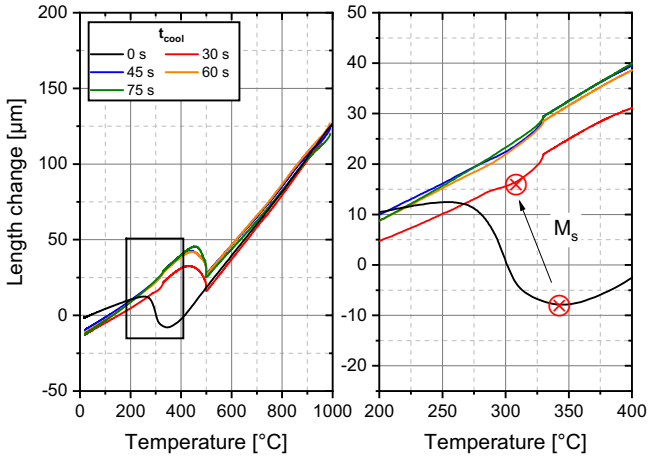

Fig. 9. Measured length change during different cooling times after short time austenitization and quenching to 500 °C.

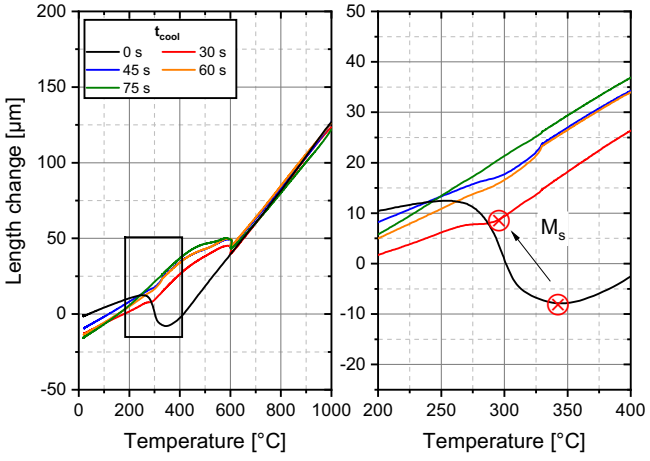

Fig. 10. Measured length change during different cooling times after short time austenitization and quenching to 600 °C.

explained with the smaller length changes during bainite formation compared to Fig. 9.

The following results of the hardness measurements (Fig. 11) and the microstructural images (Fig. 12) of the samples with a quenching temperature of 500 °C (600 °C see Appendix A) correlate very well to the described dilatation curves. Here the darker phase relates to the bainitic microstructure due to a smaller echting effect in the needle-shaped martensite. With increasing cooling times the bainite content increases and after 75 s nearly 100% bainite is formed. Comparing the microstructures of Fig. 12a and Fig. 12e, a higher bainite content after short time austenitization compared to slow heating conditions can be determined. This shows that short time austenitization speeds up the bainite formations, which can decrease the process time producing

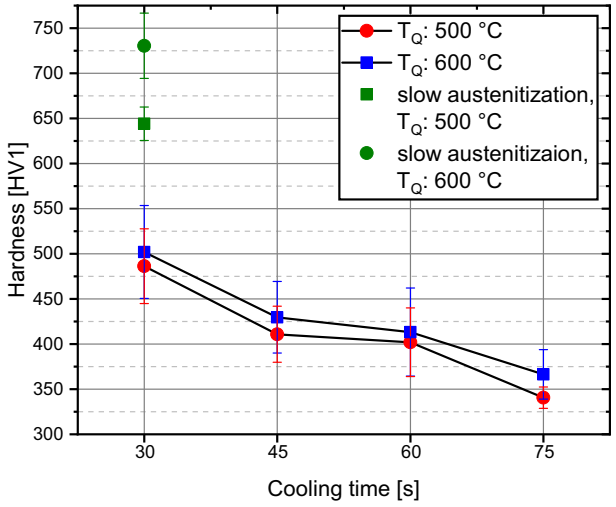

Fig. 11. Hardness of mixed bainitic martensitic microstructures after short time and slow austenitization.

mixed microstructures via induction hardening. Assuming completely dissolved carbon at 1000 °C [21] the primary cause of this is the fine austenitic microstructure after short time austenitization providing more nucleation points for the initialization of the bainitic transformation. The resulting hardness values depending on the cooling time for short time (1 s) as well as slow austenitization (60 s) are depicted in Fig. 11. Maximum values of 500 HV1 were achieved after cooling times of 30 s. The hardness increases with shorter cooling times and therefore lower bainite contents. The samples, which slowly cooled down from 600 °C, show slightly higher hardness values compared samples with $T_Q = 500$ ° C, due to higher martensite contents. A slow austenitization results in a quite higher hardness, which is comparable with the hardness of full martensitic microstructures after conventional quenching, confirming the presented micrographs.

3.2. Induction hardening experiments

3.2.1. Short time induction hardening

Fig. 13 (left) depicts the measured surface temperature histories of the short time induction hardening experiments. After reaching T_{max} the self quenching process starts while the spray moves up. Subsequently, the surface is quenched down to room temperature by the shower. The resulting hardness distribution (Fig. 13 right) displays the typical characteristics, showing a hardened surface ($HV > 800$ HV1), with an abrupt transition to the initial microstructure 270 HV1. Here it has to be stated that no tempering effects of the initial microstructure occur, due to the fact that the used steel was already in a highly tempered state. Nevertheless, in the case of the shorter austenitization time, high tensile residual stresses in sections of the initial microstrcture were measured (see Fig. 14) confirming the described problems faced by the fatigue strength. Furthermore the measured axial compressive residual stresses at a smaller hardening depth are higher than the

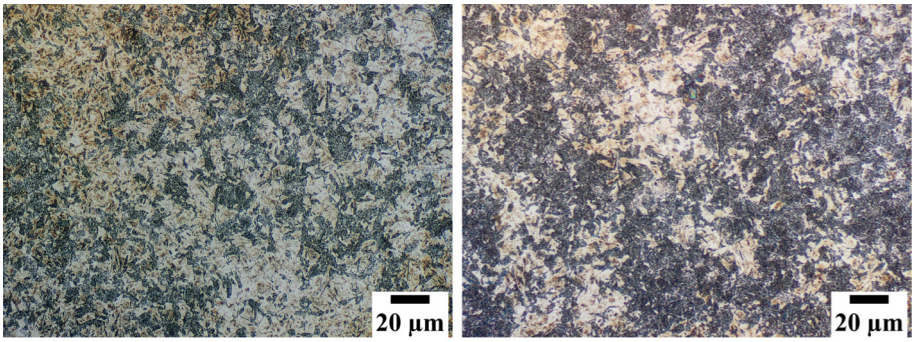

(a) 1000 °C/s to 1000 °C; t_{cool} = 30 s (b) 1000 °C/s to 1000 °C; t_{cool} = 45 s

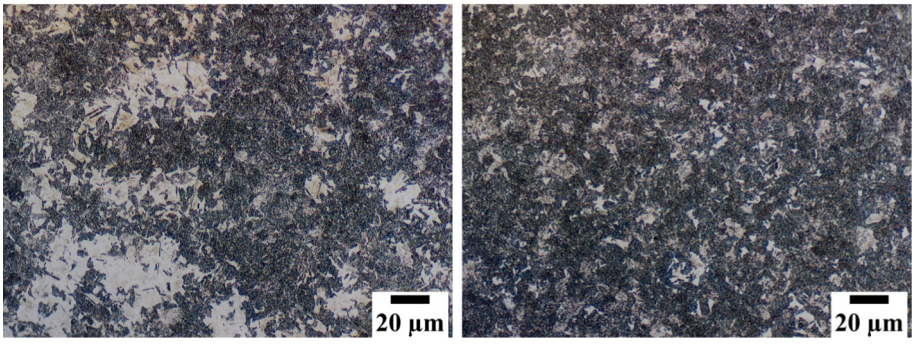

(c) 1000 °C/s to 1000 °C; t_{cool} = 60 s (d) 1000 °C/s to 1000 °C; t_{cool} = 75 s

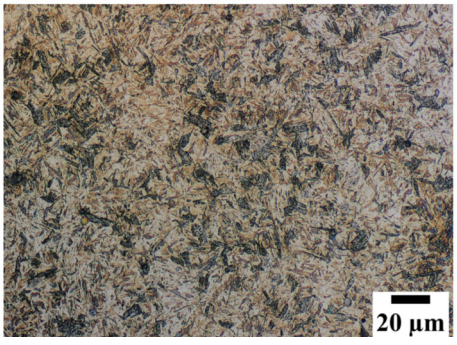

(e) 17 °C/s to 1000 °C; t_{cool} = 30 s

Fig. 12. Micrographs of the mixed microstructures after quenching to 500 °C in dependence of t_{cool}.

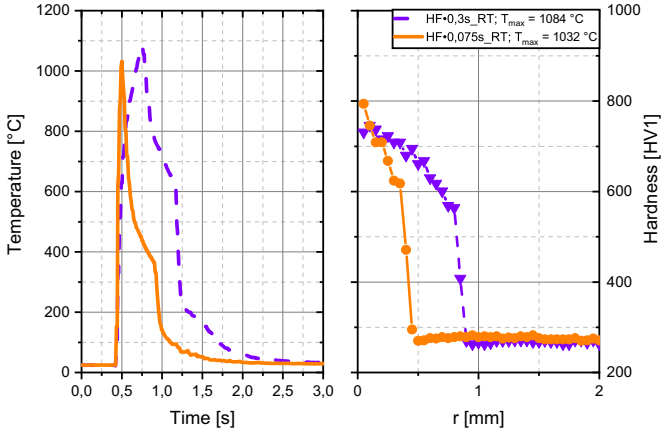

Fig. 13. Measured temperature development (left) and hardness profile (right) after short time induction hardening.

ones of the deeper hardening depth confirming the literature [9,22]. For the sake of completeness the micrographs of these experiments are attached in Appendix A.

3.2.2. Bainduction I

Due to the fact that mixed microstructures generated by dilatometry have the highest hardness values and sufficient bainite contents of around 30% after a cooling time of 30 s, the controlled *Bainduction I* experiments were carried out with the same cooling time and both quenching temperatures T_Q. Regarding the measured temperature profiles (Fig. 15 left) a slight overheating of 80 °C can be seen in the case of a quenching temperature of 500°°C. Despite using the same heating power for the first austenitization in all *Bainduction* experiments, the maximum austenitization temperature fluctuates between 1000 °C and 1080 °C. This undesired effect can be explained by communication between the hardening machine controller and the inverter which is based on a non-realtime computer hardware. Since the triggering of a

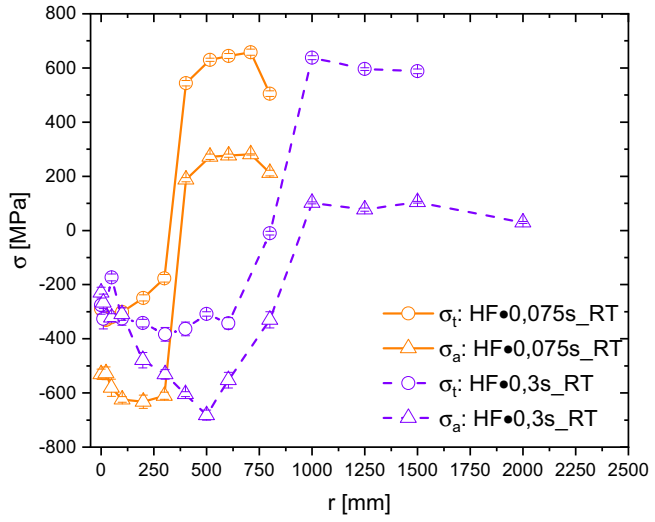

Fig. 14. Measrued depth resolved residual stresses after short time induction hardening.

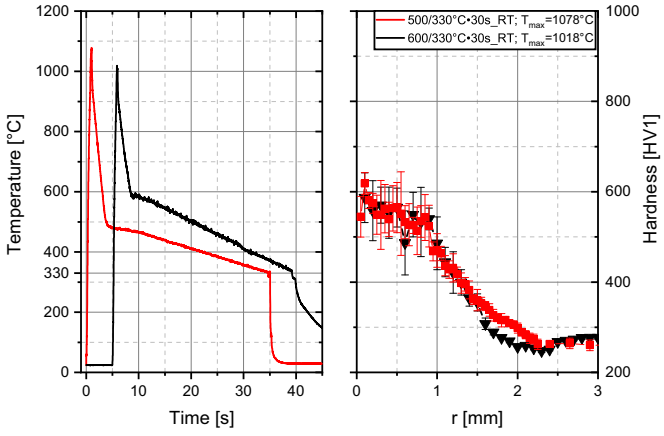

Fig. 15. Measured temperature development (left) and hardness profile (right) after the *Bainduction I* experiments.

long time process cannot be triggered by the inverter itself (as in convetional martensitic induction hardening) the heating step in the bainduction strategies exhibits a stochastic time lag (approx. 40 — 80 ms) which cannot be circumvented using the current setup. In the case of heating rates of 1000 Ks^{-1} this can lead to the shown temperature fluctuations. Furthermore the electromagnetic field could have an impact on the used thermocouples and therefore influence the measured temperature [23,24]. Nevertheless it is obvious that the desired controlled heat treatments can be implemented with the developed setup. The measured hardness (Fig. 15 right) indicates that the quenching temperature doesn't affect the hardness significantly. Compared to the dilatometric experiments higher values at the surface can be noticed. The use of another steel batch in the induction hardening experiment with a higher carbon content and different austenitization conditions could be the reason for this. The hardness is nearly constant up to a depth of 1 mm and shows high standard deviations due to the mixed microstructure. In the following the hardness decreases smoothly within 1 mm to the initial hardness. Regarding the micrographs in Fig. 16 of both states, higher bainite contents from a distance of 1 mm can be seen. This explains the smooth hardness decrease in this section and indicates an incomplete carbon solution during austenitization due to a lower maxium temperature. The smaller amount of solved carbon in turn, accelerates the bainite kinetics

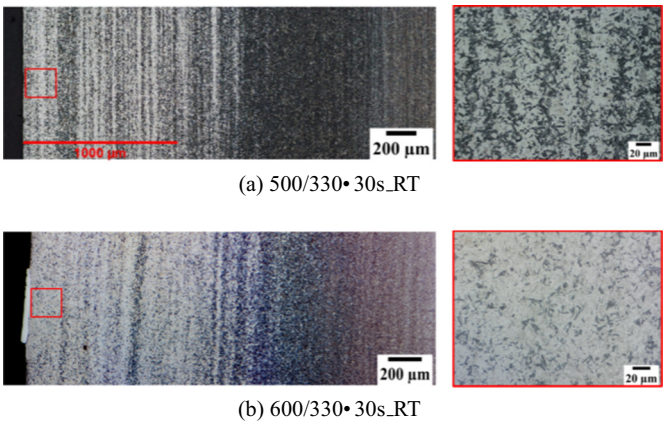

Fig. 16. Micrographs of the inductive generated mixed microstructure in the surface after the *Bainduction I* experiments.

[25,26]. Considering the bainite content in the surface after the heat treatments a good correlation with the dilatometric results can be stated, showing a faster bainite transformation with $T_Q = 500$ ° C and a bainite content of 34%. For that reason the following experiments of *Bainduction II* and *Bainduction III* base on the controlled heat treatment with $T_Q = 500$ ° C.

3.2.3. Bainduction II

After reaching a temperature of 330 °C, in this heat treatment the samples were subsequently reaustenitized up to 1000 °C. The second austenitization was hereby realized with a HF-heating pulse in 0.05 s (see Fig. 17 left). While reaching 330 °C after the controlled cooling step, a microstructure consisting of already formed bainite and retained carbon enriched austenite exists. The measured hardness indicates that the short heating impulse reaustenitizes the surface layer up to a depth of 0.75 mm. Below this the hardness decreases abruptly to a small plateau 450 HV1 similar to the hardness of the bainitic-martensitic microstructure generated as well with the *Bainduction I* strategy. Analogously, the standard deviatons increase due to a dual phase microstructure. In spite of the very short austenitization time, the former transformed bainite transforms almost completely back into austenite in the outer suface layer. This erases the generated favourable high hardness values of the mixed microstructure up to a depth of 1 mm. Fig. 18, showing the resulting microstructure, confirms the hardness profile showing three different microstructural layers up to the initial

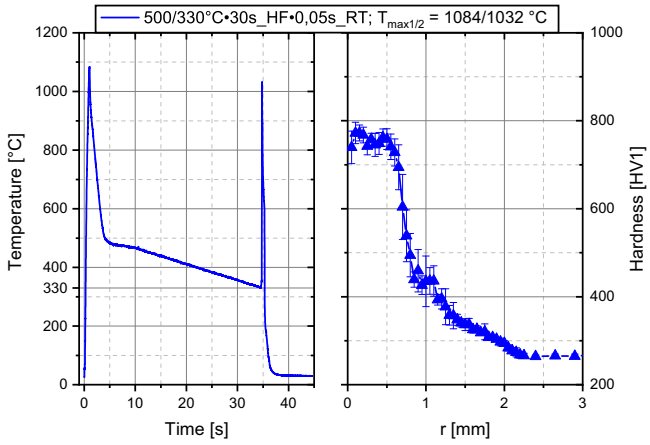

Fig. 17. Measured temperature profile (left) and hardness development (right) after the *Bainduction II* experiment.

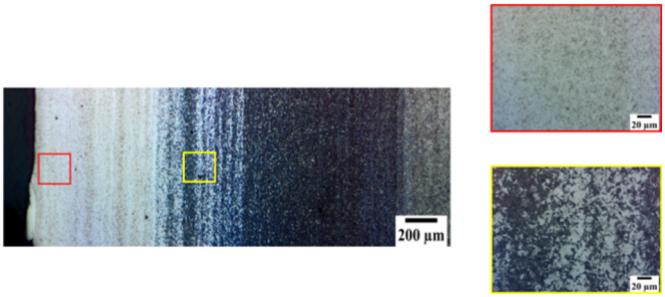

Fig. 18. Micrographs of the surface after the heat treatment strategy *Bainduction II*.

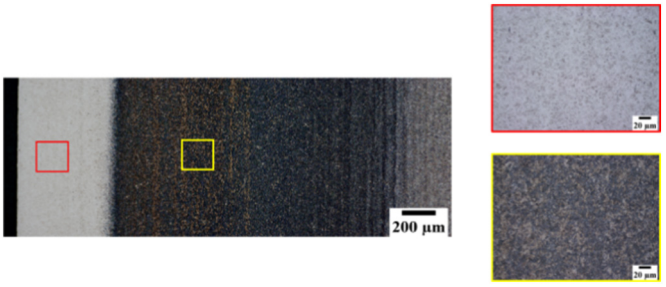

Fig. 20. Micrographs of the surface after the heat treatment strategy *Bainduction III*.

microstructure. The fully martensitic layer, which passes over into a mixed bainitic-martensitic microstructure ending in a nearly full bainitic/inhomogenous austentitized section.

3.2.4. Bainduction III

The last presented inductive heat treatment considers a short time austenitization in 0.075 s of the generated surface layer state after the *Bainduction I* treatment. In this case, considering the hardness development in Fig. 19 on the right, a similar profile compared to the one of *Bainduction II* was adjusted. Only the hardening depth of 0.5 mm is different. The reason for this effect lies in the temperature niveau of the sample, which is much higher in the case of a direct reaustenitization, leading to higher hardening depths and a smaller transition with a mixed mircrostructure. The corresponding microstructure is depicted in Fig. 20. Regarding the micrgraph of the section below the martensitic layer a mixed microstructure out of bainite and tempered martensite can be noticed. The hardness minimum at 0.6 mm of around 375 HV indicates a higher tempering state as in the deeper sections. Starting from an already completely transformed microstructure the reheating leads to tempering effects, decreasing the hardness in this region slightly. It seems that the occurring tempering effects don't have a huge impact on the initial hardness of the mixed microstructure compared to short time induction hardening.

The comparison of the residual stresses in axial and tangential direction after the three shown controlled inductive heat treatments is shown in Fig. 21. Taking the heat treatments *Bainduction I* and *Bainduction II* into regard, compressive residual stresses of around −100 MPa arise in axial direction, which increase slightly to −300 MPa. All in all nearly constant axial compressive residual stresses were measured in the up a depth of 2 mms. In contrast, the tangential component shows higher compressive residual stresses in a range of

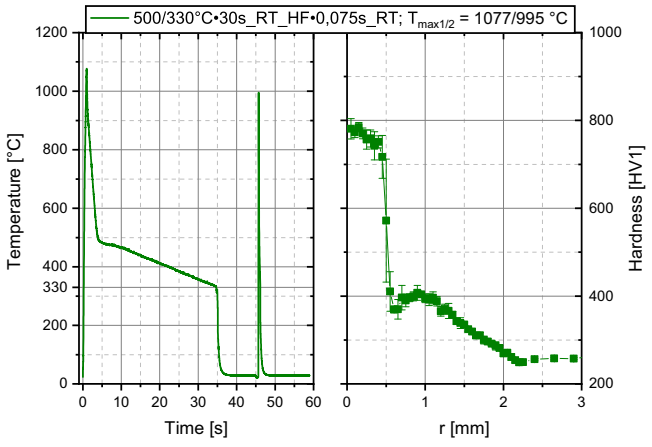

Fig. 19. Measured temperature development (left) and hardness profile (right) after the *Bainduction III* experiment.

−400 MPa to −600 MPa. Here the compressive residual stresses are greater in the case of a direct reaustenitization. It is likely that this is caused by the higher amount of martensite in the surface and therefore a larger volume increase during phase transformation inducing higher compressive stresses. The transiton from compressive into tensile residual stresses is smooth and located in the section of the mixed microtructure. Despite the sharp hardness change at a distance of 0.7 mm in the case of *Bainduction II*, the residual stresses do not behave in the same manner as it is usual after short time induction hardening. A sharp transition into tensile residual stresses can be seen for the *Bainduction III* variant. The transition depth of 400μm correlates very well with the hardness measurements and the corresponding micrograph. Consequently, the tensile residual stresses arise in the section of the mixed microstructure with a hardness of around 400 HV. Furthermore, compared to the other heat treatments, higher axial compressive residual stresses at the surface are achieved, while the tangential component shows slightly smaller values.

3.3. Simulative results

The comparison of the simulated and experimentally measured temperature developement during the *Bainduction III* process is depicted in Fig. 22 on the left. By using a constant heat transfer coefficient of 150 $Wm^{-2}K^{-1}$ for the air cooling during heating with low MF-Power a good accordance between the simulated and measured surface temperature was achieved, which verifies the temperature measurements at the surface with the used thermocouples. The chosen heat transfer coefficient corresponds very well to the literature considering the heat transfer of circulated air [27,28]. Regarding the first austenization at the surface and different subsurfaces in Fig. 22 on the right, it is obvious that a austenitization temperature of 1000 °C is not achieved in the complete heat affected surface. The simulated maximum austenitization temperatures at the different subsurfaces $T_{A,\,Max}$ (see Fig. 23 right), showing a nearly homogenous austenitization temperature up to a distance of 1 mm, correlate very well with the measured hardness profile after the *Bainduction I* process. This confirms the assumption of an inhomogenous austenitization and the resulting higher bainite contents in the subsurface (see Fig. 16). The maxmimum austenitization temperatures during the re-austenitization for the *Bainduction III* experiment are shown in Fig. 23 on the right. Here the results indicate that the remaining martensitic microstructure will be tempered at temperatures between 200 °C and 600 °C up to a depth of 1.25 mm.

3.4. Discussion

To make a statement on the surface layer states after the *Bainduction I-III* experiments with a dual phase microstructure, short time hardening experiments were carried out in such a way to allow for a comparison of the methods. As can be seen in Fig. 24a, a good comparison of the resulting hardening depth by a standard hardening experiment with a heating time of 0.3 s with the first two methods could be achieved. All

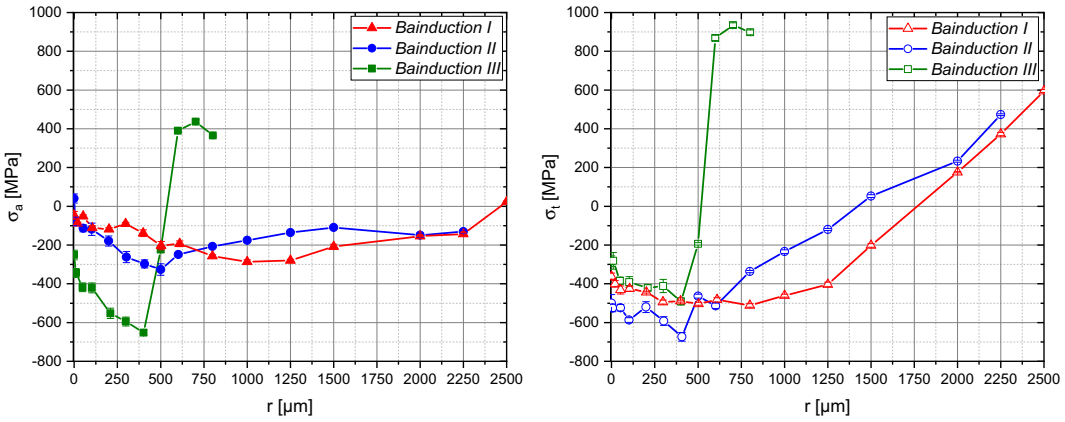

Fig. 21. Comparison of the measured residual stresses as a function a surface distance for the three controlled induction heat treatments.

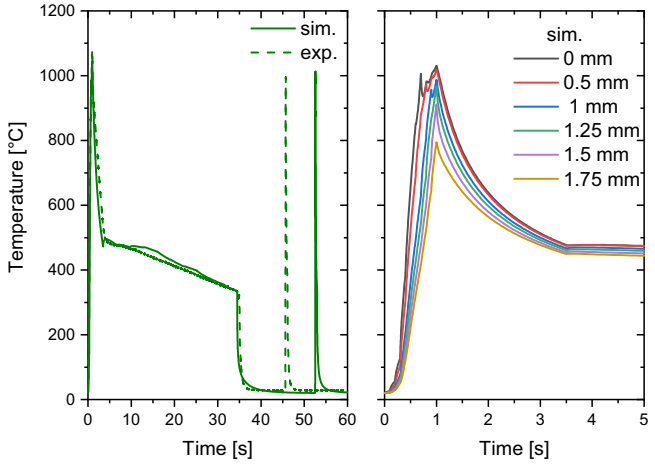

Fig. 22. Comparison of the measured and simulated temperature at the surface during the Bainduction III experiment (left) and the simulated temperature profiles in different subsurfaces (right).

three hardness profiles show a hardened surface up to 0.75 mm. Even though generating lower hardness values with a mixed microstructure, a smooth transition up to the initial microstructure was achieved, which was one goal of this study. Furthermore, considering the positive effects of a mixed microstructure in a convenient compostion shown in literature, the surface itself can also cause an improvement on the mechanical properties. A direct reaustenitization increases the maximum surface hardness by a subsequent steepening of the transition. Nevertheless higher hardness values in the transition zone are achieved compared to short time induction hardening. The second induction hardening experiment with a heating time of 0.75 s shows a similar depth of the martensitic hardened surface as the surface after a controlled cooling and a reaustenitization starting from room temperature (see Fig. 24b). In this case a previous generated mixed microstructure can increase the hardness level over 100 HV in the section where tensile stresses arise.

Considering tempering processes to reduce the tensile stresses after induction heating and also to increase the ductility, a loss of the martensite hardness is expected. This effect would also reduce the hardness of mixed microstructures. Especially the surface layer state of the *Bainduction II* variant will align the conventional hardness profile. Despite especially for the surface state with an overall mixed microstructure a tempering process needs not to be necessary due to the fact that the ductility can be adjusted by the amount of bainite. In contrast, the generated mixed microstructure of bainite and highly tempered martensite in the inner layer sections after the *Bainduction III* process is independent of further tempering processes. Therefore the high tensile residual stresses can be decreased by a tempering process without a weakening of the already highly tempered microstructure with a sufficient hardness. The only disadvantage of this strategy is a cleaning step, which is necessary before the reaustenitization. All in all these

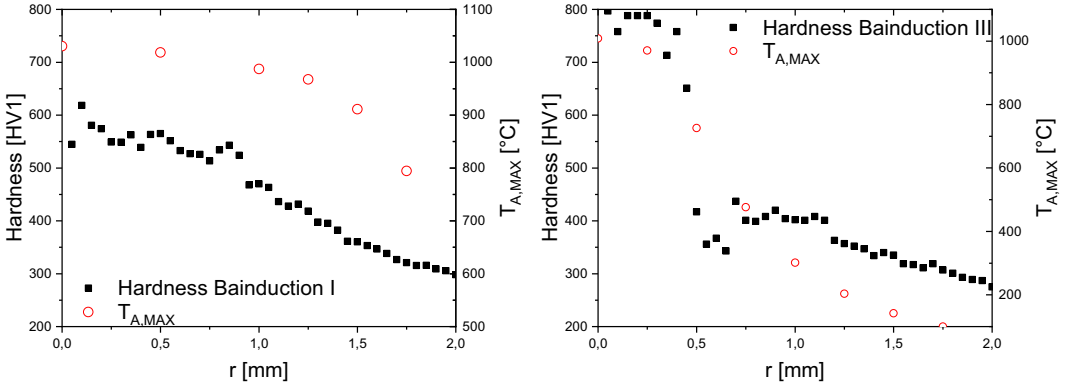

Fig. 23. Correlation of the simulated maximum austenitization temperature $T_{A,Max}$ with the measured hardness profiles after the *Bainduction I* (left) and *Bainduction III* (right) experiments.

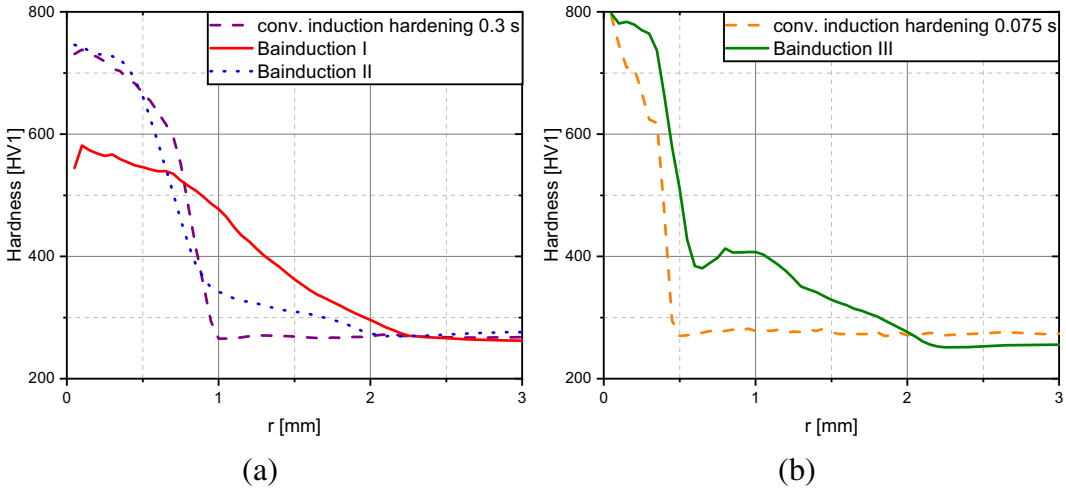

Fig. 24. Comparison of the hardness profiles after short time induction hardening and a controlled induction hardening process.

properties make the processes *Bainduction I* and *Bainduction III* very promising.

Due to the favourable compressive residual stress state in the surface of all shown heat treatment and a smooth transition into tensile residual stresses it can be assumed that the tensile residual stresses will be of minor importance considering the advantage in the fatigue strength. With this assumption and the fact that tempering will reduce the existing residual stresses, the fatigue strength is assumed to be proportional to the mechanical properties and so the hardness profile can be used as an indicator for the depth resolved fatigue strength, neglecting surface roughness effects. The estimated fatigue strength based on the hardness measurements after the conducted heat treatments is depicted in Fig. 25 and compared to possible load cases. The load cases were chosen in such a manner that failure would start in the subsurface area. In both shown load cases the *Bainduction* methods would increase the fatigue strength. Especially in the case of *Bainduction I* the fatigue strength of the mixed microstructure could even be higher when better mechanical properties can be reached due to an optimal chosen phase composition, which is neglected in the shown prediction.

4. Conclusion

An innovative induction heat treatment strategy generating bainitic-martensitic microstructures in the surface was presented. Therefore, an inductor concept was developed to ensure a controlled cooling after austenitization. The additively manufactured inductor enables a simultaneous air cooling during heating. Based on dilatometric tests, different heat treatment strategies were designed. Hereby it was found that a short austenitization time fastens the bainite kinetics. Furthermore a carbon enrichment in the austenite while creating 30% bainite was detected. This in turn can lead to a higher martensite hardness as described in literature [11,13]. All developed *Bainduction* heat treatment strategies, which include a generation of a mixed microstruture with a controlled cooling, were sucessfully implemented and the desired bainite content in the mixed microstructure was adjusted in the aimed range. Nevertheless the shown results indicate that further improvements of the process control and hardening machine hardware should be realized to increase the process stability. On the one hand the temperature measurement should be conducted with a pyrometer instead of thermocouples. By integrating a pyrometer into the inductor, the rotation of the samples, decreasing circumferential temperature inhomogeneities, would be enabled and possible impacts of the electromagnetic field on the thermocouple could be eliminated. On the other hand the fluctuations of the first austenitization temperature have to be eliminated to get more stable and reproducible austenitization conditions. This could be done by a revision of the internal timer of the generator. Subsequent hardness measurements as well as residual stress analyses were done to compare the new heat treatment with standard inductive heat treatments. The results showed that comparable compressive residual stresses as well as a strengthening of the microstructure in the transition zone was achieved. The typical abrupt decrease of hardness and the residual stresses was smoothened which can lead to a improvement of the fatigue strength. Another positive effect is that with the shown innovative heat treatment strategies and the strengthening effects, subsequent tempering processes, reducing tensile residual stresses, are not absolutely essential and could be obmitted in a production chain of induction hardened parts. All in all the presented work provides a promising approach to improve the surface layer state of induction hardened parts by extending the process opportunities. In the context of controlled cooling after induction heating various research questions arise and can be investigated further using the developed device:

- The influence of high heating rates during austenitization on a subsequent bainite formation should be regarded in detail to allow a simulative prediction and optimization of the shown heat treatment strategies.

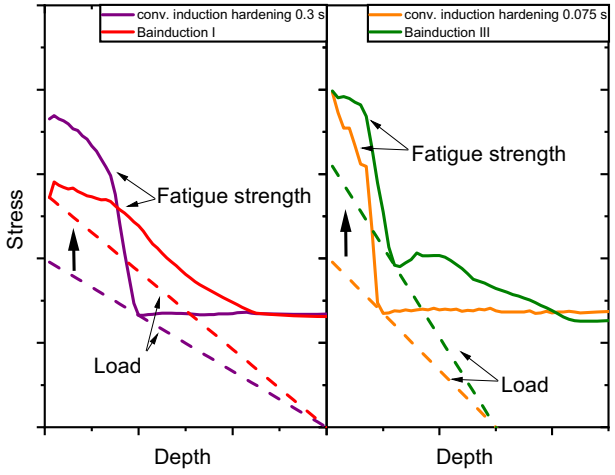

Fig. 25. Illustration of possible improvements of the fatigue strength due to a tailored bainitic-martensitic microstructure via a controlled induction surface hardening derived from [9].

- As shown in the present work promising mixed microstructures can be generated. The charaterization of their mechanical and fatigue properties have to be done, to quantify the possible improvements.
- The component performance in dependence of the different surface states, which differ in microstructure, hardness as well as in the residual stress state, must be investigated in order to give a complete picture of the benefits incorporated by this specialized process.

Data availability statement

The data that support the findings of this study are available from the corresponding author, [F. Mühl], upon reasonable request.

Declaration of competing interest

The authors declare that they have no known competing financial interests or personal relationships that could have appeared to influence the work reported in this paper.

Acknowledgement

This research was supported by the Dr.-Ing. Willy-Hoefler-Stiftung as part of the project “Tailored bainitic-martensitic microstructures by means of inductive surface hardening for AISI4140”. The authors also want to thank Mr. A. Haeussler of IDEA GmbH for helping in the development and manufacturing of the presented inductor concept.

Appendix A

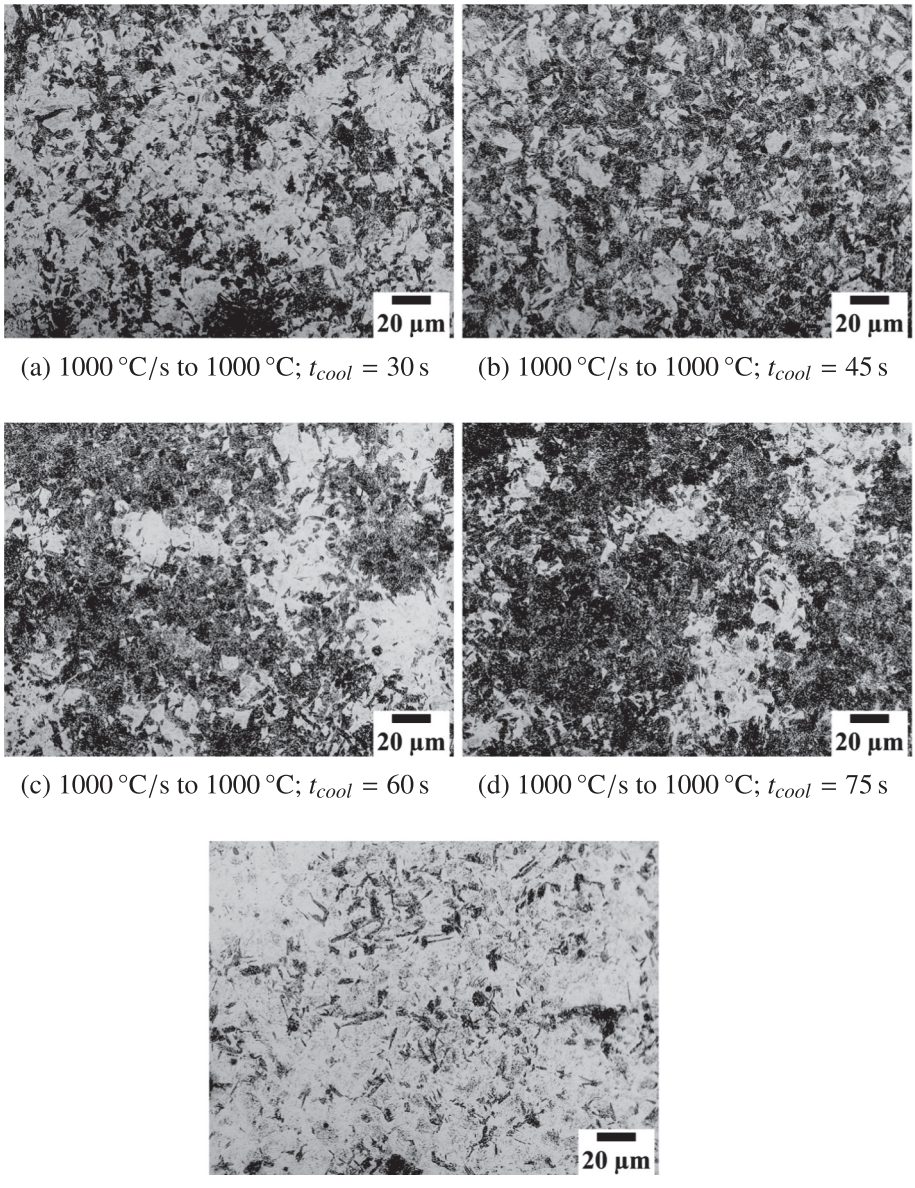

(a) 1000 °C/s to 1000 °C; t_{cool} = 30 s (b) 1000 °C/s to 1000 °C; t_{cool} = 45 s

(c) 1000 °C/s to 1000 °C; t_{cool} = 60 s (d) 1000 °C/s to 1000 °C; t_{cool} = 75 s

(e) 17 °C/s to 1000 °C; t_{cool} = 30 s

Fig. A1. Micrographs of the mixed microstructures after quenching to 600 °C in dependence of t_{cool}.

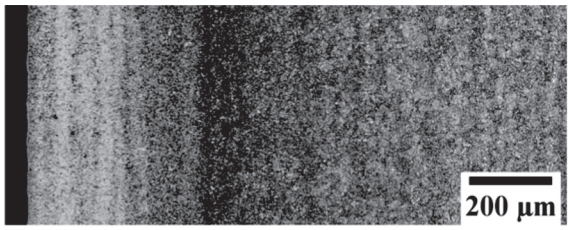

(a) HF•0.075 s_RT

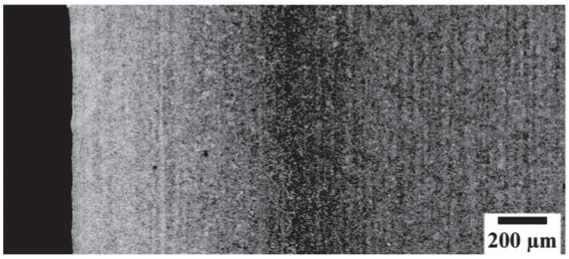

(b) HF•0.3 s_RT

Fig. A2. Micrographs of the surface after conventional induction hardening.

References

[1] H. Berns, W. Theisen, Eisenwerkstoffe - Stahl und Gusseisen, Springer-Verlag, Berlin, Heidelberg, 4., bearb. Aufl., 2008

[2] G. Hanisch, Qualität von induktionshärteprozessen und -anlagen in der serienfertigung, HTM Härtereitechn. Mitt. 61 (2) (2006) 71–75.

[3] G. Conradt, Randschichthärten von kurbelwellen, MTZ – Motortechn. Z. 64 (9) (2003) 746–751.

[4] G. Benkowsky, Induktionserwärmung: Härten, Glühen, Schmelzen, Löten, Schweißen, Verl. Technik, Berlin, 5., stark bearb. Aufl., 1990

[5] M. Schwenk, Entwicklung und Validierung eines numerischen Simulationsmodells zur Beschreibung der induktiven Ein- und Zweifrequenzrandschichthärtung am Beispiel von vergütetem 42CrMo4, 2012.

[6] J. Komotori, M. Shimizu, Y. Misaka, K. Kawasaki, Fatigue strength and fracture mechanism of steel modified by super-rapid induction heating and quenching, Int. J. Fatigue 23 (2001) 225–230.

[7] D. Kaiser, J. Damon, F. Mühl, B. de Graaff, D. Kiefer, S. Dietrich, V. Schulze, Experimental investigation and finite-element modeling of the short-time induction quench-and-temper process of aisi 4140, J. Mater. Process. Technol. 279 (2020) 116485.

[8] F. Nazemi, J. Hamel-Akré, P. Bocher, Modeling of cementite coarsening during tempering of low-alloyed-medium carbon steel, J. Mater. Sci. 53 (8) (2018) 6198–6218.

[9] P. Braisch, J. Rollmann, Werkstoffkundliche gesichtspunkte zur beurteilung des schwingfestigkeitsverhaltens induktiv randschichtgehärteter bauteile, Mater. Werkst. 31 (1) (2000) 66–80.

[10] D. Kaiser, Experimentelle Untersuchung und Simulation des Kurzzeitanlassens unter Berücksichtigung thermisch randschichtgehärteter Zustände am Beispiel von 42CrMo4, Phd thesis Karlsruhe Institute of Technology, 2019.

[11] Y. Tomita, K. Okabayashi, Improvement in lower temperature mechanical properties of 0.40 pct c-ni-cr-mo ultrahigh strength steel with the second phase lower bainite, Metall. Trans. A. 14 (2) (1983) 485–492.

[12] Y. Tomita, K. Okabayashi, Heat treatment for improvement in lower temperature mechanical properties of 0.40 pct c-cr-mo ultrahigh strength steel, Metall. Trans. A. 14 (11) (1983) 2387–2393.

[13] c. H. Young, H.K.D.H. Bhadeshia, Strength of mixtures of bainite and martensite, Mater. Sci. Technol. 10 (3) (1994) 209–214.

[14] J. Chen, B. Zhang, Effect of bainite volume fraction on fatigue properties of bainite/martensite dual phase ea4t steel, J. Miner. Metal Mater. Eng. (2019) 12–21.

[15] J. Wen, Q. Li, Y. Long, Effect of austempering on microstructure and mechanical properties of a gcr18mo steel, Mater. Sci. Eng. A 438-440 (2006) 251–253.

[16] A. Morri, L. Ceschini, M. Pellizzari, C. Menapace, F. Vettore, E. Veneri, Effect of the austempering process on the microstructure and mechanical properties of 27mncrb5-2 steel, Arch. Metall. Mater. 62 (2) (2017) 643–651.

[17] S.M.C. van Bohemen, Bainite and martensite start temperature calculated with exponential carbon dependence, Mater. Sci. Technol. 28 (4) (2012) 487–495.

[18] M. Habschied, S. Dietrich, D. Heussen, V. Schulze, Performance and properties of an additive manufactured coil for inductive heat treatment in the mhz range, HTM J. Heat Treat. Mater. 71 (5) (2016) 212–217.

[19] DIN-Normenausschuss Eisen und Stahl, Din en iso 683–2 für eine wärmebehandlung bestimmte stähle, legierte stähle und automatenstähle –teil 2: Legierte vergütungsstähle, 2018-09-00.

[20] B. Eigenmann, E. Macherauch, Röntgenographische untersuchung von spannungszuständen in werkstoffen. tl. 3, Mater.-Wiss. Werkstofftech. 27 (1996) S.426–437.

[21] T. Miokovič, J. Schwarzer, V. Schulze, O. Vöhringer, D. Löhe, Description of short time phase transformations during the heating of steels based on high-rate experimental data, J. Phys. IV Proc. 120 (2004) 591–598.

[22] H. Fahry, H.-W. Zoch, H. Schlicht, Enstehung von eigenspannungen und verzügen bei der induktiven randschichthärtung von bauteilen, Härterei-Techn. Mitt. (44) (1989) 149–156.

[23] A. Smalcerz, R. Przylucki, Impact of electromagnetic field upon temperature measurement of induction heated charges, Int. J. Thermophys. 34 (4) (2013) 667–679.

[24] S. Beguš, J. Bojkovski, J. Drnovšek, G. Geršak, Magnetic effects on thermocouples, Meas. Sci. Technol. 25 (3) (2014) p. 035006.

[25] J. Damon, F. Mühl, S. Dietrich, V. Schulze, A comparative study of kinetic models regarding bainitic transformation behavior in carburized case hardening steel 20mncr5, Metall. Mater. Trans. A 50 (1) (2019) 104–117.

[26] S.M.C. van Bohemen, J. Sietsma, Modeling of isothermal bainite formation based on the nucleation kinetics, Int. J. Mater. Res. 99 (7) (2008) 739–747.

[27] J. Jan, M. Nannapuraju (Eds.),CFD Investigation of Quench Media and Orientation Effects on Structural Stress Induced in the Intense Quenching Processes for Aluminum Cylinder Heads, 2017.

[28] B. Xiao, G. Wang, R.D. Sisson, Y. Rong, L. Canale, S.W. Dean, Influencing factors of heat transfer coefficient in air and gas quenching, J. ASTM Int. 8 (4) (2011) p. 103403.